SCANNING Vol. 4, 131–140 (1981)

Received: March 24, 1981

Original Paper

Direct SEM Study of Frozen Inner Ear

E. R. Lewis and J. B. Pawley*

Donner Laboratory, University of California, Berkeley, CA 94720, USA
* Present address: HVEM Laboratory, University of Wisconsin, Madison, WI 53706, USA

Introduction

The inner ear of the vertebrates provides exquisite sensitivity to linear and rotational motion, to tilt with respect to the gravitational vector, to airborne sound, and, in certain lower vertebrates, to substrate-borne vibration (*Lowenstein* and *Roberts* 1950). With these sensitivities, the sensory organs of the ear serve as crucial elements in orientational, postural, and eye-movement control systems as well as in communication systems and predator avoidance systems in man and other vertebrates. The special, selective sensitivities of each individual inner-ear sensory organ undoubtedly are attributable to a great extent to the specialized acellular structure that overlies its sensory epithelium. In the semicircular canal the acellular structure (the cupula) takes the form of a diaphragm, which is deformed by motion of the fluid, induced by angular acceleration (*McLaren* and *Hillman* 1977). In the otoconial or otolith organs (i.e., the saccule, the utricle, or the lagena) the acellular structure (the otoconial or otolithic membrane) has calcium carbonate crystals that serve as inertial masses and move in response to linear accelerations or to shifts in orientation with respect to the gravitational vector (*Marco* et al. 1971). In auditory organs, the acellular structures (tectoria) take various shapes from species to species and in some cases may be largely responsible for frequency selectivity.

Functional variations among the afferent nerve fibers from the ear go well beyond the major sensitivity divisions listed in the previous paragraph. Among the fibers exhibiting response to acceleration, for example, one finds some that show nearly constant response (constant frequency of nerve impulses) to constant acceleration and others that adapt to constant acceleration, thus showing maximum response to *changes* in acceleration (*Fernandez* et al. 1972). Among the latter, the dynamics and the steady-state level of adaption vary considerably from fiber to fiber. Both adapting and nonadapting fibers tend to respond in direct proportion to acceleration above a certain threshold level. The constant of proportionality and the threshold level of acceleration both vary considerably from fiber to fiber. Such variations in response properties reflect significant gradations of function within individual organs of the ear and, therefore, have been of great concern to students of the auditory and vestibular systems. Although several alternative possibilities exist, it is very reasonable to expect that these functional gradations at least in part are attributable to morphological gradations in the cupula, tectorium, or otoconial membrane and its mechanical coupling to the underlying sensory cells (hair cells).

Because of their high water content, cupulae, tectoria and otoconial membranes are extraordinarily susceptible to shrinkage during normal histological procedures. Gross distortion occurs in response to osmication, to dehydration for embedding or drying, and to critical-point or freeze drying (*Lewis* and *Pawley* 1979). Subtle changes even have been observed in response to isomotic changes in the ionic milieu (*Kronester-Frei* 1978). In order to study the morphology of these acellular structures and expose their linkages to underlying hair cells, one somehow must fracture or section the tissue in the plane normal to the sensory epithelium. One would like to do this in a way that avoids the gross distortion inflicted by dehydration or drying, so neither sectioning of embedded tissue nor cryofracturing followed by critical-point or freeze-drying is appropriate. Thus the acellular structures of the inner ear are prime candidates for cryo-

fracture followed by direct SEM observation of the frozen tissue (*Pawley* and *Norton* 1977). In the study described in this paper, we made such direct observations on two otoconial organs of the inner ear of the bullfrog (*Rana catesbeiana*), the utricle and the lagena.

Basic Methods

Unfixed or very lightly glutaraldehyde-fixed sensory epithelium was dissected from the inner ear and trimmed to remove all extraneous tissue. The tissue was placed against filter paper to remove excess water then very quickly mounted with a very small amount of silicone-based bath caulking compound on a thin copper disc.

As soon as it was mounted, the tissue was thrust with precooled forceps into liquid nitrogen that had been supercooled by boiling under vacuum. Once frozen, the tissue was stored under liquid nitrogen until we were ready to fracture and observe it. At that time, the disc and tissue were mounted, still under liquid nitrogen, on a precooled specimen stub, which in turn was transferred in a precooled carrier to a special vacuum chamber attached directly to an SEM (*Pawley* and *Norton* 1977, *Pawley* et al. 1978). In the chamber, the stub was screwed firmly into a shuttle that was held automatically at a temperature level below 100 K. Once in the chamber, the tissue remained under a vacuum of 2×10^{-7} mbar while it was fractured, etched if necessary, evaporatively coated with gold (15–25 nm), and observed. To prevent formation of frost on the tissue, the sample was almost completely surrounded by a cold shroud at all times. The tissue was fractured with a precooled knife oriented so as to induce free fracture through the tissue. The silicone caulking compound which is rigid at these temperatures, served to hold the tissue in place against the shearing force required to generate a free fracture. Fracturing was observed with a 10–60 × binocular microscope mounted over a glass window in the chamber ceiling; and once a satisfactory free fracture was obtained, the tissue was transferred on the shuttle to a cooled copper block that could be tilted and rotated during evaporative coating. After being coated with gold, the specimen was transferred on the shuttle directly into the cold stage of the SEM, which was held at approx. 100 K.

In some cases, after fracturing but before coating, the tissue was subjected to freeze-etching. This was accomplished by resistive heating of the shuttle itself as well as by radiant warming of the specimen by means of a 3.5 W resistive heating element mounted approximately 1 cm above the specimen stub. Depending on the depth of etch desired, etch times varied from 1–5 min or more. The temperature of the specimen surface during etching could not be determined, but the shuttle and stub temperature was monitored and typically reached approximately 173 K at the end of the etch cycle which was terminated by discontinuation of the electrical power to heating elements and reactivation of the shuttle cooling process. For more detailed descriptions of the etching and coating apparatus the reader should see *Pawley* et al. 1980.

Direct Observation of Unetched Fracture Surfaces

It is well known that cryofracture surfaces tend to form along specific structures (such as lipid membranes) in biological specimens (*Southworth* et al. 1975). In our SEM studies of inner-ear tissue, we have found that this tendency occasionally leads to macroscopic landmarks in free-fracture surfaces, and that such landmarks may provide clues to structural relationships. For us, they served the equally important function of providing orientation. For example, the structures in Fig. 1 are granules (presumably associated with the superficial pigmentation found in the frog inner ear) and transected myelinated nerve fibers; both are consistent indicators that the location is the outer surface of the labyrinth (the structure in which the sensory organs reside). The structures in Fig. 2 are nuclei and apical surfaces of epithelial cells, which indicate that the location is the inner surface of the labyrinth.

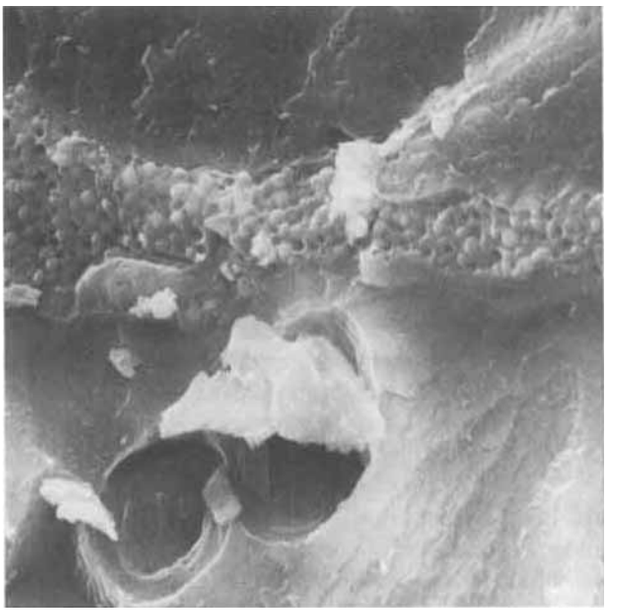

Fig. 1 Unetched freeze fracture through the membranous labyrinth of the inner ear of the bullfrog, viewed in the frozen state. Numerous pigment granules and two transected myelinated nerve fibers (partially obscured by debris) indicate that the location is near the outer surface of the labyrinth wall. Horizontal field width = 38 μm.

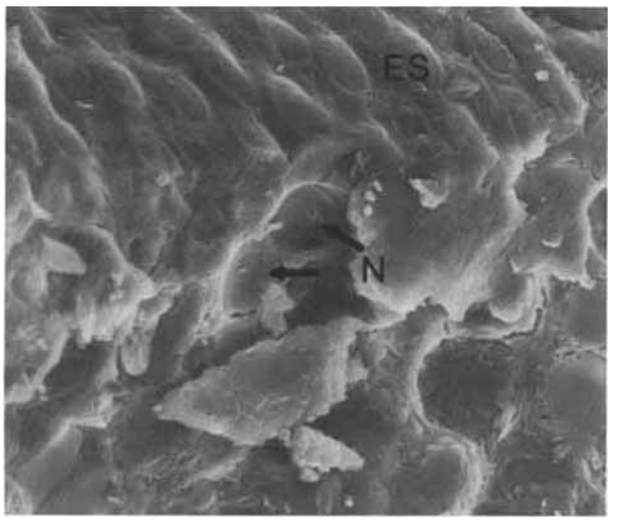

Fig. 2 Unetched freeze fracture near the inner surface of the labyrinth wall. Cleavage has ocurred partially over the tile-like epithelial surface (ES) and partially over the surfaces of nuclei (N). Horizontal field width = 34 μm.

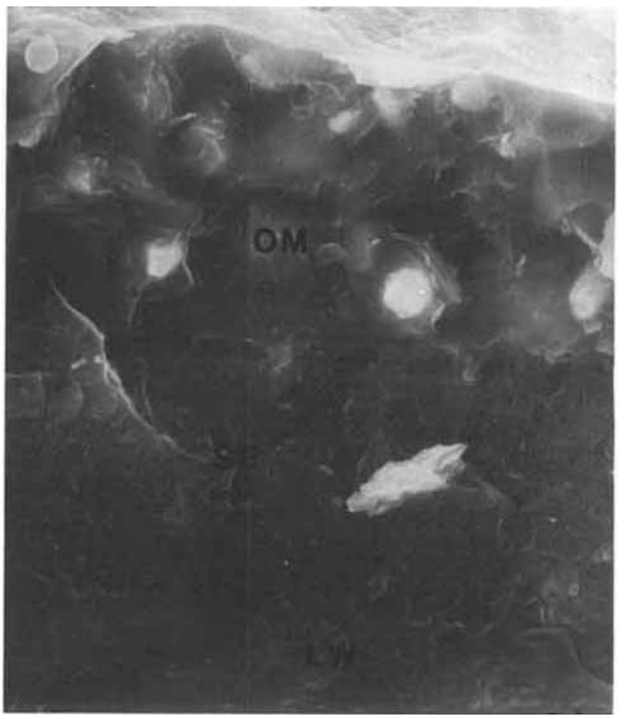

Fig. 4a

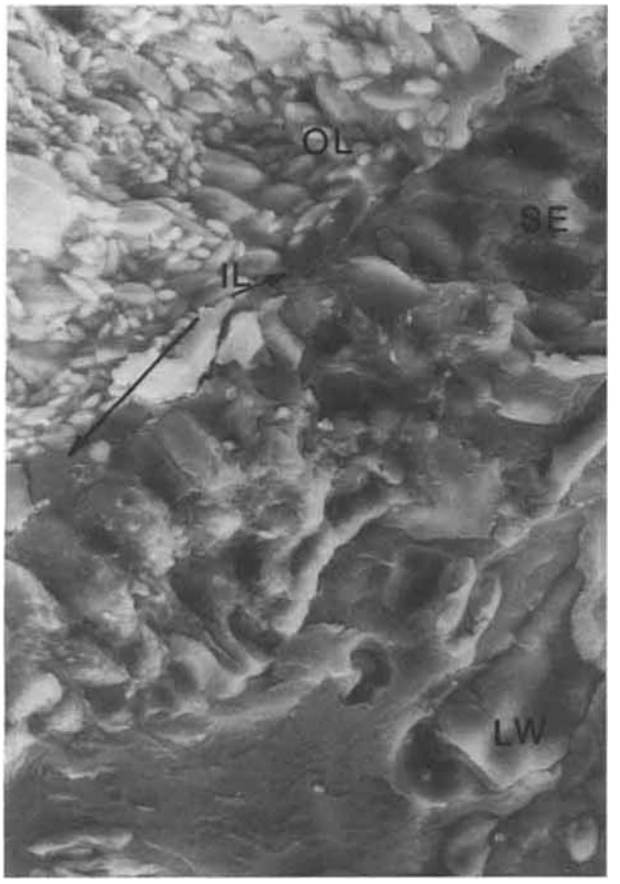

Fig. 3 Unetched freeze fracture through the sensory surface of the lagena, showing the following layers in cross-section: labyrinth wall (LW), sensory epithelium (SE), inner layer (IL) and otoconial layer (OL) of the otoconial membrane. Horizontal field width = 281 μm.

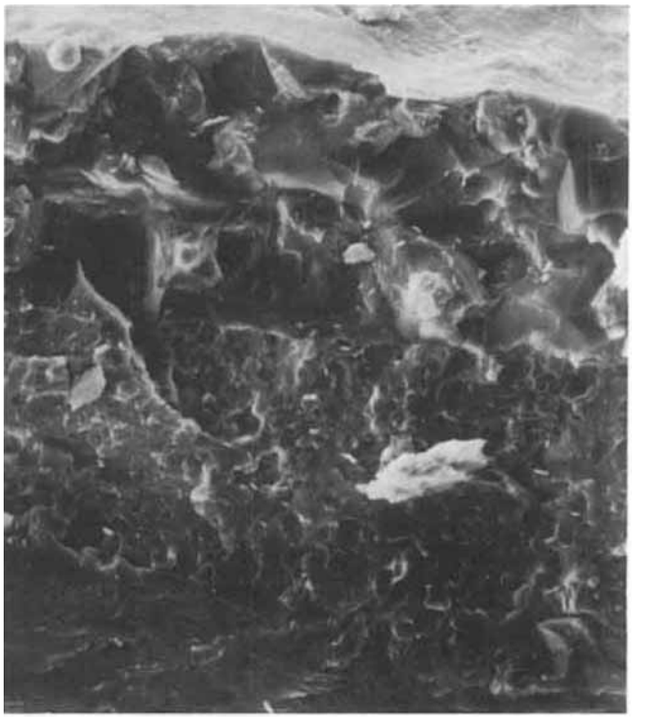

Fig. 4b

Fig. 4 Unetched freeze fracture through the sensory surface of the utricle. Textural differences between the fracture surfaces through labyrinth wall (LW), sensory epithelium (SE), and otoconial membrane (OM) are more clearly visible in Fig. 4b, taken at an accelerating potential of 10 kV, than they are in Fig. 4a, taken at 30 kV. Horizontal field width = 88 μm.

A second, more consistent clue to structural relationships over our unetched fracture surfaces was provided by variation of surface texture. In Fig. 3, for example, one can distinguish four layers in the vicinity of the sensory surface of the lagena, an inner-ear organ sensitive to tilt and to vibration in lower vertebrates. At the bottom is the cartilagious labyrinthine wall, the fracture surfaces through which generally are smooth. Next is the sensory epithelial cell layer, which has a fractured surface that generally is rough and exhibits depressions or protuberances corresponding to cleavage over nuclei. Above the epithelial layer is a second smooth layer, which corresponds to the inner region of the otoconial membrane. Next is the outer region of the otoconial membrane, the cleavage through which is made very rough by the presence of calcium carbonate (aragonite) crystals.

In these studies we wished to determine the thicknesses of the various layers of the otoconial membrane, and variations of those thicknesses from place to place in the lagena and the utricle. As a result of the variations in surface texture, we were able to make some of the necessary measurements on unetched fracture surfaces.

The appearance of surface texture depended markedly on the beam accelerating voltage, and the variation often could be enhanced for the viewer by observation at reduced voltage. In Fig. 4, for example, one can distinguish three layers in the vicinity of the sensory surface of the utricle, an organ sensitive to tilt. At the bottom is the relatively smooth fracture surface through the labyrinthine wall; next is the relatively rougher fracture surface through the epithelial cell layer; and at the top is a jagged but otherwise smooth

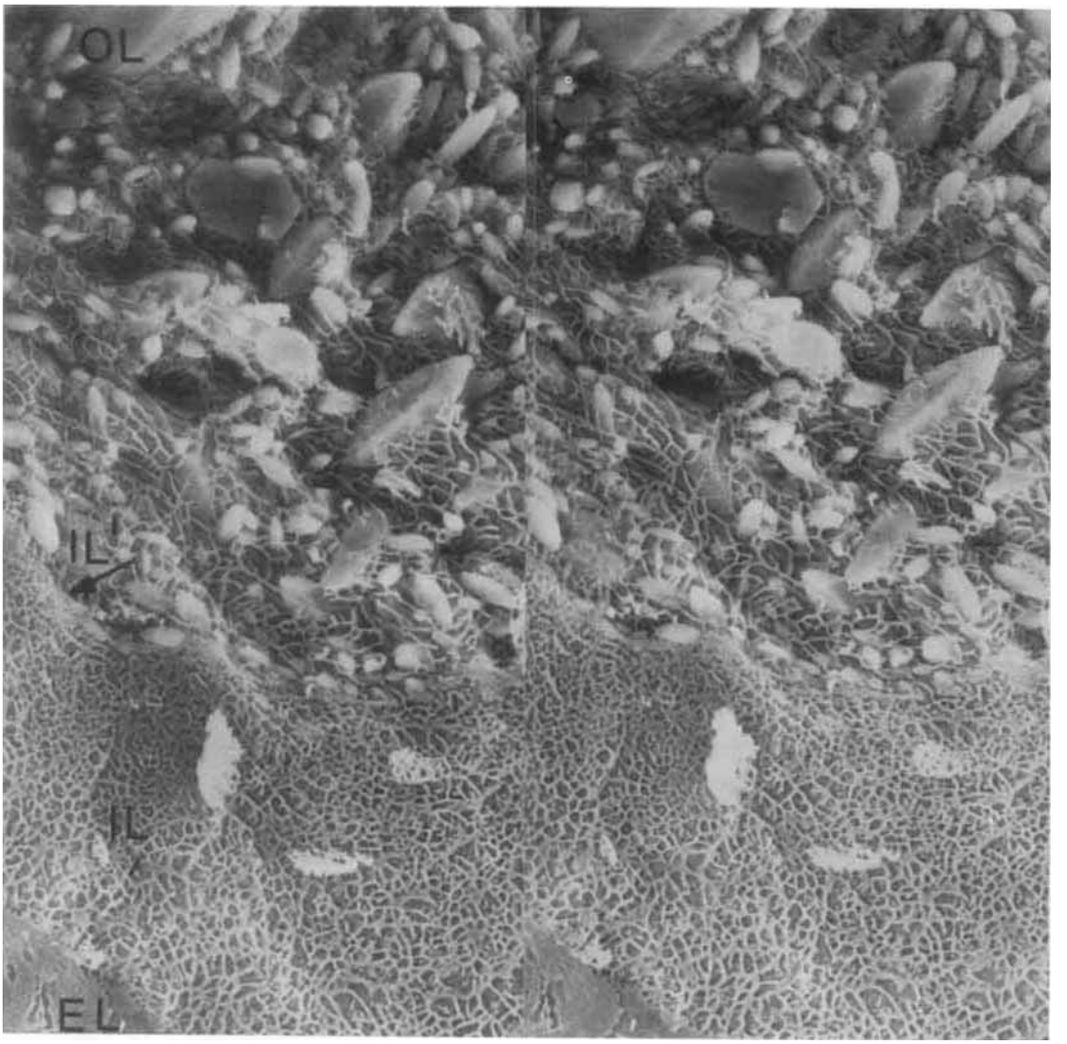

Fig. 5 Moderately etched freeze fracture through the sensory surface of the lagena, showing the otoconial layer (OL), the intermediate acellular layer (IL'), the inner acellular layer (IL), and the epithelial layer (EL). Horizontal field width = 51 μm.

fracture surface through the otoconial membrane. The appearances of the individual layers are quite different in Fig. 4a, which was taken with 30kV accelerating voltage, and Fig. 4b, which was taken with 10kV, even though the range of contrast in the two images is approximately the same.

Freeze Etching

The distinctions between the various layers were made more prominent by moderate to deep freeze-etching, as illustrated in Fig. 5 and 6. The otoconial layers (at the top of each figure) were made more obvious in part by the exposure of the otoconial crystals themselves. However, the limits of that and the other layers were sharpened for the most part as a result of ice crystal artifacts. Many of the regions of interest in the sample very likely were too far (100 μm or more) from the surface to permit cooling sufficiently rapid to avoid such artifacts. Furthermore, since etching was accomplished by warming of the tissue to temperatures above the recrystalization temperature of ice, extensive crystalization undoubtedly occurred during that

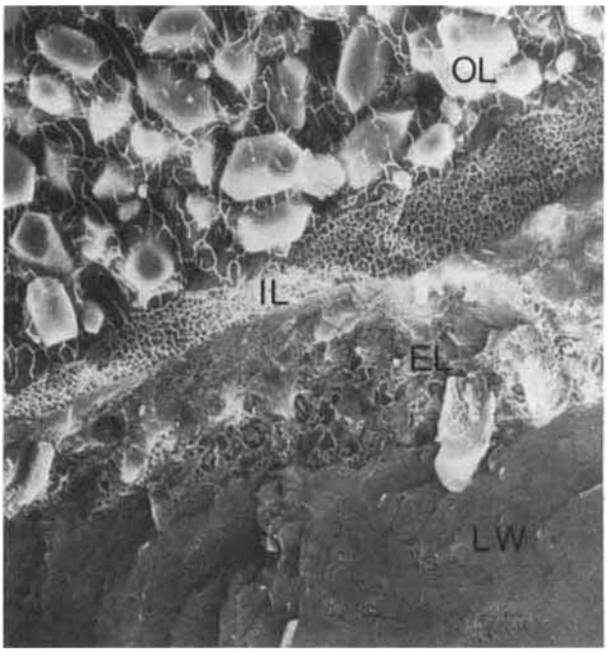

Fig. 6 Moderately etched freeze fracture through the sensory surface of the utricle, showing the otoconial layer (OL) and inner layer (IL) of the otoconial membrane, the epithelial layer (EL), and the labyrinth wall (LW). Horizontal field width = 100 μm.

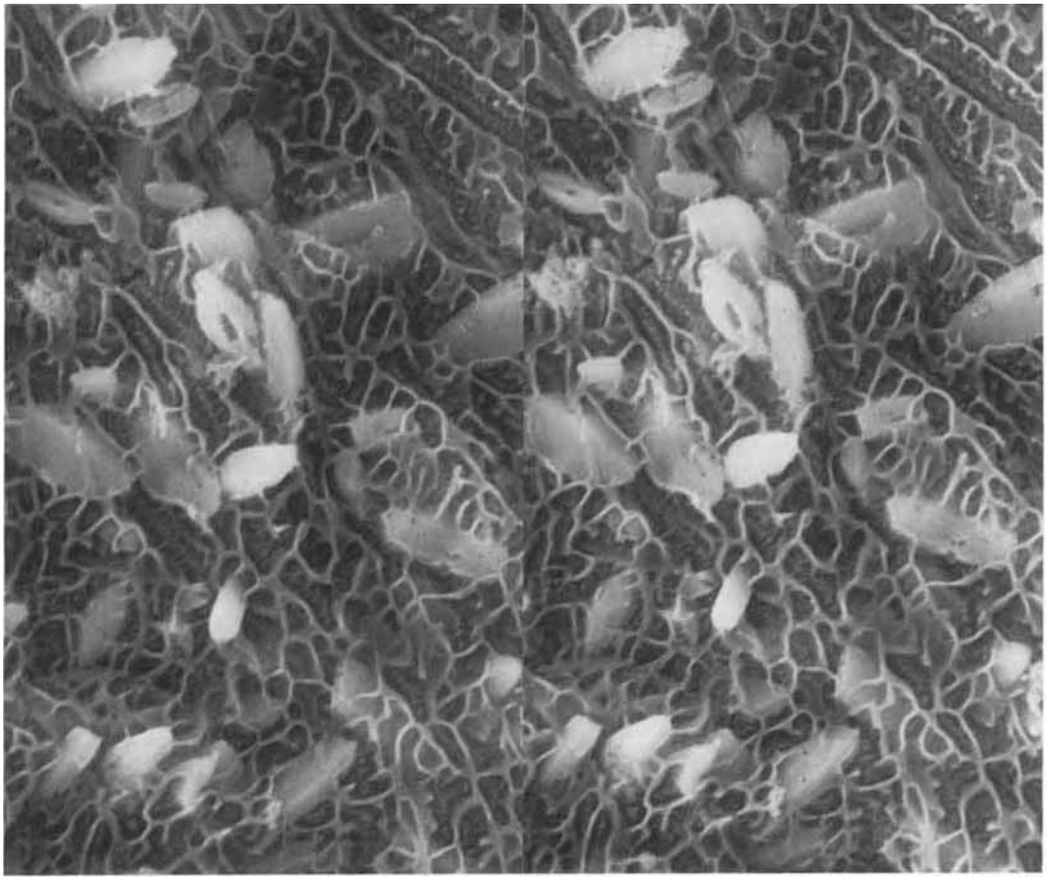

Fig. 7 Stereomicrograph of the otoconial layer, showing details of the eutectic margins. Horizontal field width = 23 μm.

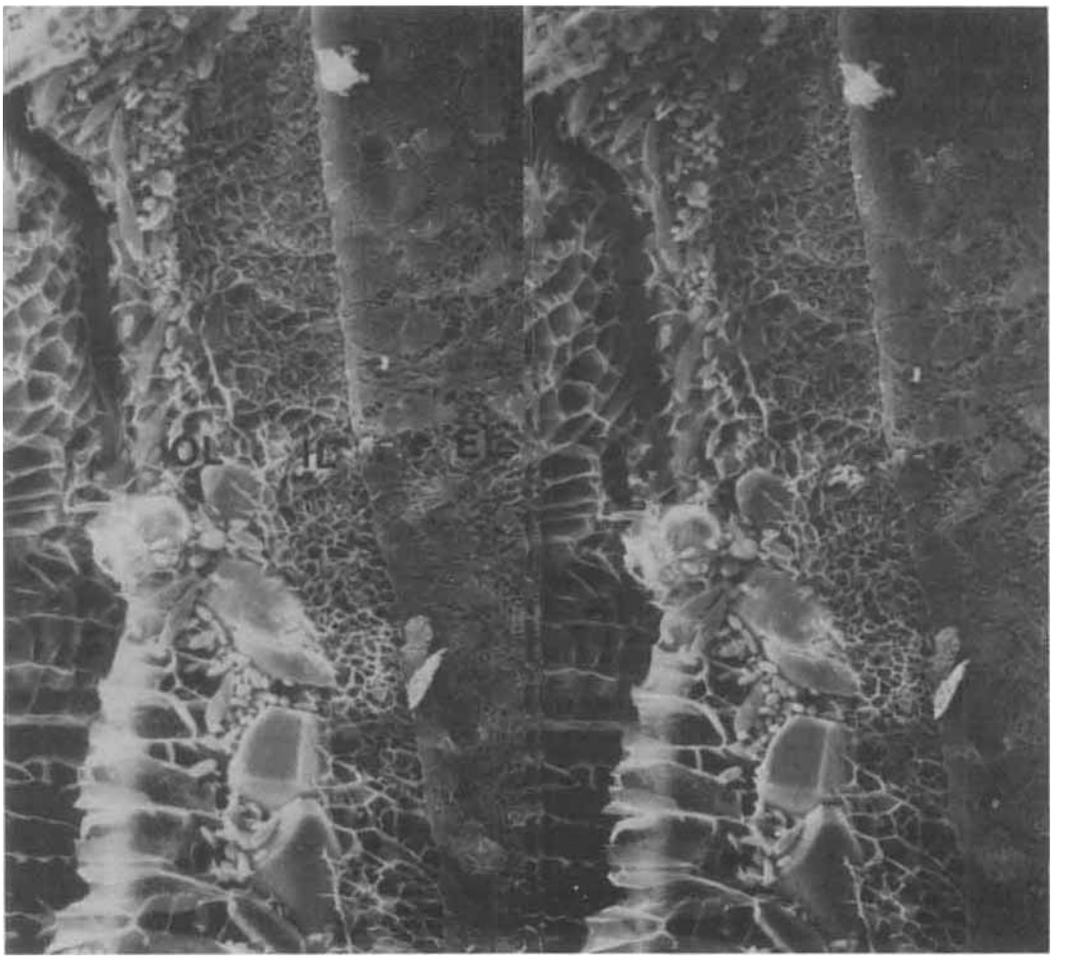

Fig. 8 Stereomicrograph of a deep-etched freeze fracture through the anterior edge of the utricular sensory surface, showing the epithelial layer (EL), the inner acellular layer (IL), the otoconial layer (OL), and a layer of ice (I) adjacent to the surface. Horizontal field width = 108 μm.

process as well. However, this artifact has advantages as well as disadvantages. The size of the crystals in a given region depends on the number of crystals there and this in turn depends on water content and the concentration of potential ice-nucleation centers (e.g., organic macromolecules that tend to bind large quantities of water) as well as on the cooling rate. Under freeze etch, the crystal size is revealed by the spacing of the eutectic margins, the regions where solutes collect as they are frozen out of the forming crystals (Fig. 7) (*Miller* 1979, *Staehelin* and *Bertrand* 1971). One would suppose that eutectic margins would tend to be most widely spaced in regions with the highest water content and the lowest concentration of organic macromolecules. This supposition has been confirmed by *Steere* and *Erbe* 1977, with freeze-etched agar and acrylamide gels, and by *Echlin* et al. 1979, in duckweed. Thus, the markedly different spacings of eutectic margins from region to region in Figs. 5 and 6 apparently reflect differences in molecular content among the various layers in the vicinity of the sensory surface.

Under deep etching, the spacing of the eutectic margins increased in the acellular layers, and the boundaries between those layers became less sharp. Comparing Figs. 6 and 8, for example, one can see that the boundary between the otoconial layer (the layer with calcium carbonate crystals) and the acellular layer just beneath has lost definition under deep etch in the utricle. On the other hand, deep etching reveals clearly certain cellular structures that either were obscure or not visible at all under moderate etch. For our purposes, the most important of these structures were the cilia and specialized microvilli (stereocilia) that project from the apical surfaces of the receptor cells and presumably make contact with the otoconial membrane (Fig. 9). *Hudspeth* and *Cory* 1977 and others have demonstrated that it is a shearing motion of the stereocilia that elicits a response in the receptor cell. Another major objective of this study is to determine the relationships between the arrays of stereocilia and the various layers of the otoconial membrane, thereby to understand better the mechanical linkages involved in sensory transduction. Obser-

Fig. 9 Stereocilia of a single sensory receptor cell of the utricle, revealed by deep etching. Horizontal field width = 7.1 μm.

vations of deep-etched tissue have been very useful in this regard, especially when combined with observations of unetched and moderately-etched tissue.

Problems in Measuring Layer Thickness

Parameters of special interest to us were the thicknesses of the various layers of the otoconial membranes. Since we were attempting to infer these thicknesses from fracture surfaces through the layers, we faced the common geometric problems associated with sectioned tissue. The problems were different in the two organs, and the solution in each case was facilitated by stereomicrography.

The wall of the lagena is a nearly perfect hemisphere, and the layers of the otoconial membrane can be considered as hemispherical shells. Taking the region of the fracture surface where measurement is made to be part of a plane extending through the hemisphere, as shown in Fig. 10a, and assuming that the SEM electron beam is normal to that plane, the apparent thickness (t_a) of the shell is given in normalized form by the following expression:

$$\hat{t}_a = (1-\hat{h}^2)^{1/2} - [(1-\hat{t})^2 - \hat{h}^2]^{1/2} \qquad (1)$$

where $\hat{t}_a = t_a/t$; $\hat{h} = h/r$; and $\hat{t} = t/r$, r being the outside radius of the shell, t being the thickness of the shell measured along a radius (the standard thickness of a shell), and h being the closest distance between the plane of fracture and the spherical center. For a shell that is thin relative to its outer radius, which is true of the layers of interest to us, the relative error (ε) in the measurement of thickness

$$\varepsilon = (\hat{t}_a/\hat{t}-1) \qquad (2)$$

takes the following values as a function of $\hat{h}$:

$\hat{h}$ =	0.1	0.2	0.3	0.4	0.5	0.6	0.7
ε =	0.005	0.021	0.048	0.091	0.155	0.250	0.400

Therefore, if the fracture plane passes within the mid-

Fig. 10a ▽

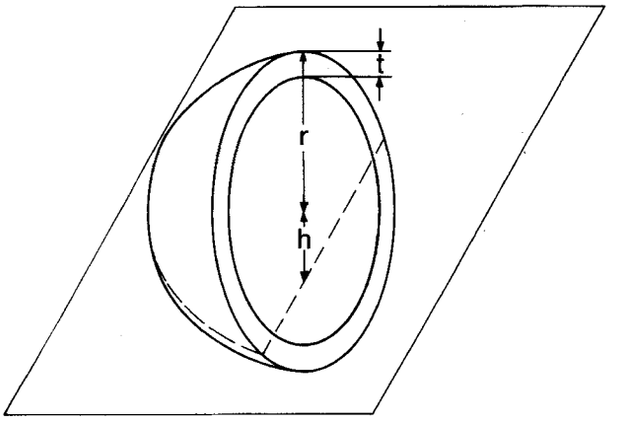

Fig. 10b ▽

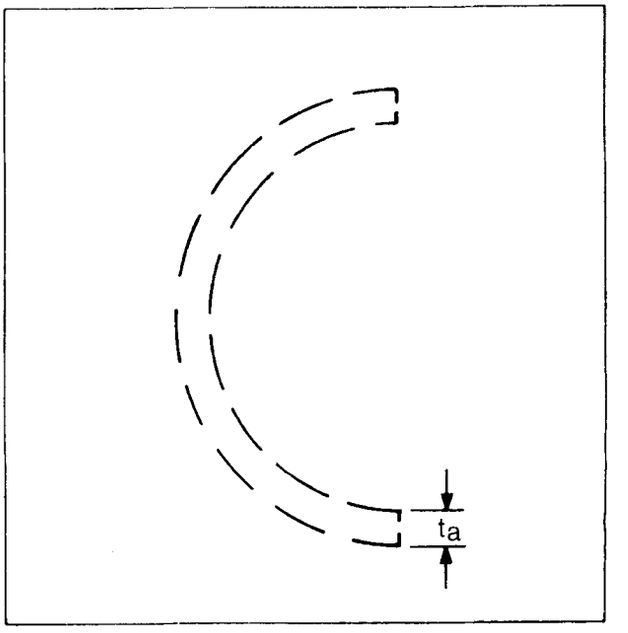

Fig. 10 Illustration of the problem of measuring the otoconial layer thicknesses in the lagena. (a) depicts the lagena as a hemispherical shell, transected by an imaginary fracture plane. (b) depicts the transected shell as it would be viewed in the fracture plane, with the plane oriented normal to the line of sight.

dle 40% of the hemisphere the error for thin shells is less than 10%. When the beam is not normal to the fracture plane, further error (ε')

$$\varepsilon' = (\cos[\Theta] - 1) \quad (3)$$

is introduced, where Θ is the angle of the electron beam with respect to a plane tangent to the shell at the point of measurement. In terms of the two error terms, the apparent thickness is related to the standard thickness by

$$t_a = t(1 + \varepsilon)(1 + \varepsilon') \quad (4)$$

so the two error components are additive only when they are small. The second error term takes on the following values as a function of tilt:

Θ =	10°	20°	30°	40°	50°
ε' =	−0.015	−0.060	−0.134	−234	−0.357

When the tilt of the beam is less than 25°, the second error term is less than 10%. Since the error introduced as a result of tilt is negative while that introduced as a result of off-center fracture is positive, we are guaranteed to have error less than 10% if the fracture surface lies within the central 40% of the hemisphere and the beam tilt is less than 25°. Since error up to 10% was quite acceptable for our purposes, we had only to judge with stereoscopic micrographs whether or not these rather generous fracture-plane and beam tilt tolerances were met. Using this method, we were able to obtain consistent measurements from specimen to specimen, indicating that our ability to judge the position of the fracture surface and beam tilt was sufficiently good.

In the case of the utricle, the layers of the otoconial membrane are nearly planar sheets. The apparent thickness (t_a) of such a sheet, viewed in the scanning electron microscope (SEM), is given by

$$t_a = t \cos(\xi - \Theta)/\cos(\xi) \quad (5)$$

where t is the thickness of the sheet measured along the line normal to the plane of the sheet (the standard thickness of a sheet); ξ is the angle of the fracture plane relative to a line normal to the plane of the sheet (i.e., $\xi = 0$ corresponds to a fracture plane perpendicular to the plane of the sheet, $\xi = 90°$ corresponds to a fracture plane parallel to the plane of the sheet); and Θ is the angle of the electron beam with respect to the plane of the sheet (see Fig. 11). The relative error (ε) in the measurement of thickness.

$$\varepsilon = (t_a/t - 1) \quad (6)$$

takes on the values given in Table 1 as a function of the two angles (ξ and Θ).

Table 1 Values of ε as a Function of ξ and Θ

Θ	ξ = 0°	10°	20°	30°
0°	0	0	0	0
10°	0.015	0.048	0.085	0.131
20°	0.064	0.137	0.227	0.347
30°	0.155	0.285	0.462	0.732

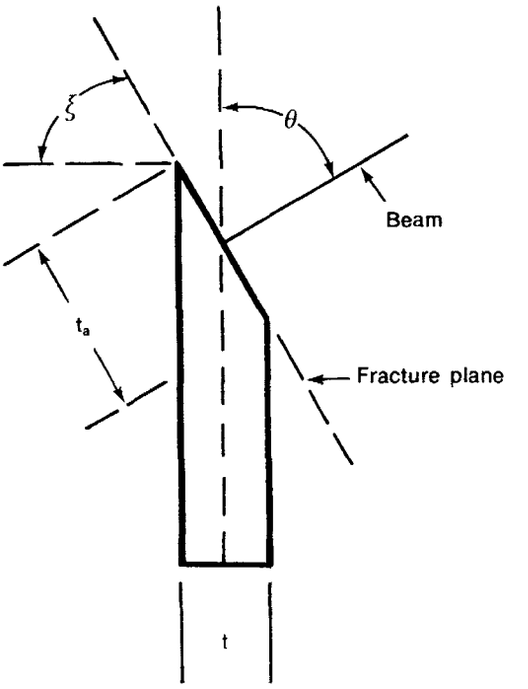

Fig. 11 Illustration of the problem of measuring the otoconial layer thicknesses in the utricle (see text for details).

Clearly, the relative error is a very sensitive function of both angles. For error less then 10%, the values of ξ and Θ are as follows: for ξ equals 0°, 10°, 20°, 30°, and 45° respectively, the maximum allowable values of Θ are 25°, 17°, 12°, 8°, and 5° respectively.

At first glance, it would appear to be very difficult to meet these tolerance limits, even with steroscopic micrographs. However, it is remarkably easy to null the angle Θ very precisely when the plane of the sheet is exposed and visible, as it is in the case of the utricle. In fact there are very sensitive monocular clues by means of which one can adjust Θ, as one easily can demonstrate by viewing a stiff card edge-on with one eye and then tilting it slightly. Once again, therefore, we were able to obtain consistent measurements of layer thicknesses from specimen to specimen.

Observations and Discussion on the Otoconial Membrane

Under both moderate and deep freeze etch, the otoconial membrane of the bullfrog lagena exhibited three distinct layers:

1. an outer, otoconial layer, with wide spacing of the eutectic margins and numerous calcium carbonate crystals,
2. an inner, acellular layer, with more narrow eutectic spacing than the otoconial layer and devoid of calcium carbonate crystals, and

3. a thin layer between the other two, devoid of crystals and (even under deep etch) exhibiting extremely narrow eutectic spacing, comparable to the spacing in the cellular layer.

The thick inner and outer layers are clearly visible in the micrograph of Fig. 5, which was taken near the edges of the sensory surface and the otoconial membrane. The intermediate layer is especially thin at the edge, but can be seen clearly on the left-hand side of the figure. Toward the center of the sensory surface, this layer is more variable in thickness and occasionally exhibits projections well into the inner layer, toward the epithelium. Over the entire sensory surface, the otoconial layer exhibited a thickness of approximately 140 μm, while the inner layer exhibited a thickness of approx. 30 μm, except where projections from the intermediate layer invaded it. Under deep etch, the cilia and sterocilia of receptor cells were seen to project into the inner layer but did not reach the intermediate layer or appear to contact its projections. The cilia of a very small population of receptor cells near the center of the sensory surface are approx. 30 μm long and presumably are capable of reaching the intermediate layer (*Lewis* and *Li* 1975). However, to date we have not been able to observe the projections of these long cilia in our freeze-fracture preparations.

Under moderate and deep freeze etch, the otoconial membrane of the bullfrog utricle exhibited only two distinct layers:

1. the outer, otoconial layer, and
2. the inner, acellular layer.

Both layers are evident in Figs. 5 and 8. The thickness of the otoconial layer ranged from approx. 25 mm to approx. 40 μm. Except at the anterior margin of the sensory surface, the thickness of the inner layer was nearly constant at approx. 16 μm. At the anterior margin, it expanded to approx. 30 μm and then tapered to zero. Inside the anterior margin, the otoconial layer exhibited a row of exceptionally large crystals, which is apparent in Fig. 8. Large crystals of this type are common in utricular otoconial membranes and occur over a band of exceptionally large receptor cells, with exceptionally long cilia and sterocilia (*Lindeman* 1969). In the present studies we have found that adjacent to that band in the bullfrog utricle, the inner layer of the otoconial membrane exhibits the same thickness (approx. 16 μm) that it does over the rest of the sensory surface. Deep etch reveals that the utricular hair cells project into the inner layer of the otoconial membrane, but not through it to the otoconial layer.

In the bullfrog saccule, the otoconial layer is more than 1 mm thick; previous studies have provided convincing evidence that the intermediate layer of the otoconial membrane of that organ is thick and contacts directly the cilia of the receptor cells (*Hillman* 1969, *Hillman* and *Lewis* 1971). The present studies indicate that the utricle and the lagena both are quite different from the saccule in that regard. It now is known that the lagena and utricle of the bullfrog both are predominantly sensors of tilt with respect to the gravitational vector or of slow linear motions, whereas the bullfrog saccule is a sensor of substrate-borne vibrations (*Baird* 1979, *Baird* et al. 1980). Ontogenetically, the lagena is derived from the saccule, whereas the utricle is derived separately, in an entirely different part of the ear (*Larsell* 1938). With respect to the organization of the otoconial membrane and its relationship to the sensory cilia and stereocilia, the bullfrog lagena appears to be intermediate between the saccule and the utricle, exhibiting an otoconial layer much thinner than that of the saccule and only a thin remnant of the intermediate layer. Thus, the lagena and the utricle apparently have converged both in morphology and in function. In addition to its sensitivity to tilt and slow linear motion, the lagena also exhibits sensitivity to vibration. It has been shown by *Baird* et al. 1980, that this sensitivity is confined to a very small population of receptor cells in the center of the sensory surface. These cells are similar to those of the sacculus, but their cilia are not sufficiently long to contact the intermediate layer.

Discussion of Methods

Although the unetched fracture surfaces in this study were very useful for determination of the thicknesses of the otoconial layers and the combined inner and intermediate layers, they did not allow us to distinguish between the last two or to observe the relationship between the arrays of cilia and stereocilia and the various layers. Moderate etching allowed us to distinguish all three layers of the otoconial membrane, but deep etching was required in order to reveal the arrays of cilia and stereocilia. Ice-crystal artifacts, which were especially disruptive in the acellular regions, totally obscured any fine structure that may have existed within the various layers of the otoconial membrane. On the other hand, these same artifacts provided marked contrast between the layers themselves, and therefore were useful. Furthermore, the sizes of the ice crystals, as revealed by the eutectic margins after freeze etching, appear to be directly related to the concentration of organic macromolecules capable of forming centers of crystalization. If they are, we can draw conclusions concerning the relative abundance of such molecules in the various layers. Ice-crystal size in extracellular regions also has been found to be related to the distance from the freezing surface (*Ornberg* and *Reese* 1979). In initially homogeneous solutions, ice crystals are smallest immediately adjacent to the freezing surface; and they become progressively

larger as one moves farther from that surface, apparently reflecting the time required to pass below the recrystalization temperature during the freezing process. In the present study, the gradation of ice-crystal size in the extracellular regions did not follow that pattern at all. The largest crystals occurred immediately adjacent to the freezing surface, in ice formed by remnants of the buffer solution adhering to the tissue. The next largest crystals occurred in the otoconial layer, which always was the layer of the otoconial membrane closest to the freezing surface. The smallest crystals were found in the intermediate layer, next to the otoconial layer; and in the inner layer were crystals much larger than those of the intermediate layer but clearly smaller than those of the otoconial layer. Thus, some factor other than distance from the freezing surface was the predominant determinant of ice-crystal size. Presumably that factor was concentration of organic macromolecules.

Acknowledgement

We thank Greg Hook and Eve Kermit for technical assistance during this research, and we are especially grateful to Professor Thomas L. Hayes of the Donner Laboratory, University of California, Berkeley, for kindly allowing us to use his AMR 1000-LaB_6 SEM equipped with BioChamber. The instrument is supported in part by the Division of Biomedical and Environmental Research of the U.S. Department of Energy. The research was supported by the National Institutes of Health, Grant NS12359 from the National Institute of Neurological and Communicative Disorder and Stroke.

References

Baird R A: Correspondences between structure and function in the bullfrog utricle and lagena. Neurosci Abstr 5, 15 (1979)

Baird R A, Koyama H, Leverenz E L, Lewis E R: Functions of otoconial and auditory organs of the bullfrog inner ear identified with intracellular dye. Neurosci Abstr 6, 223 (1980)

Echlin P, Pawley J B, Hayes T L: Freeze-fracture scanning electron microscopy of *Lemma minor* (Duckweed). Scanning Electron Microscopy 1979/III, SEM Inc, Chicago, 69–76 (1979)

Fernandez C, Goldberg J M, Abend W K: Response to static tilts of peripheral neurons innervating otolith organs of the squirrel monkey. J Neurophysiol 35, 978–997 (1972)

Hillman D E: New ultrastructural findings regarding a vestibular ciliary apparatus and its possible functional significance. Brain Research 13, 407–412 (1969)

Hillman D E, Lewis E R: Morphological basis for a mechanical linkage in otolithic receptor transduction in the frog. Science 174, 416–419 (1971)

Hudspeth A J, Cory D P: Sensitivity, polarity, and conductance change in the response of vertebrate hair cells to controlled mechanical stimuli. Pro Natl Acad Sci USA 74, 2407–2411 (1977)

Kronester-Frei A: Sodium dependent shrinking properties of the tectorial membrane. Scanning Electron Microscopy 1978/II, SEM Inc, Chicago, pp 943–948 (1978)

Larsell O: The differentiation of peripheral and central acoustic apparatus in the frog. J Comp Neurol 60, 473–527 (1938)

Lewis E R, Li C W: Hair cell types and distributions in the otolithic and auditory organs of the bullfrog. Brain Research 83, 35–50 (1975)

Lewis E R, Pawley J B: SEM freeze-fracture studies of the otoconial membrane of the frog lagena. Scanning Electron Microscopy 1979/III, SEM Inc, Chicago, pp 955–961 (1979)

Lindeman H H: Studies on the Morphology of the Sensory Regions of the Vestibular Apparatus, Springer-Verlag, Berlin pp 83–92 (1969)

Lowenstein O E, Roberts T D: The equilibrium function of the otolith organs of the thorn back ray (*Raja clavata*). J Physiol 110, 392–415 (1950)

Marco J, Sanchez-Fernandez J M, Rivera-Pomar J M: Ultrastructure of the otoliths and otolithic membrane of the macula utriculi in the guinea pig. Acta Otolaryngol 71, 1–8 (1971)

McLaren J W, Hillman D E: Displacement of the semicircular canal cupula during sinusoidal rotation. Neurosci Abstr 3, 544 (1977)

Miller K R: Artifacts associated with the deep-etching technique. In: Freeze Fracture: Methods, Artifacts, and Interpretations, (Ed. Rash J E and Hudson C S). Raven Press, New York, 31–36 (1979)

Ornberg R L, Reese T S: Artifacts of freezing in *Limulus* amebocytes. In: Freeze Fracture: Methods, Artifacts, and Interpretations, (Ed. Rash J E and Hudson C S). Raven Press, New York, 31–36 (1979)

Pawley J B, Hayes T L, Hook G R: Preliminary studies of coated complementary freeze-fractured yeast membranes viewed directly in the SEM. Scanning Electron Microscopy 1978/II, SEM Inc, Chicago, pp 683–714 (1978)

Pawley J B, Hook G, Hayes T L, Lai C: Direct scanning electron microscopy of frozen-hydrated yeast. Scanning 3, 219–226 (1980)

Pawley J B, Norton J T: A chamber attached to the SEM for fracturing and coating biological samples. J Microsc 112, 169–182 (1977)

Southworth D, Fisher K, Branton D: Principles of freeze-fracturing and etching. In: Techniques of Biochemical and Biophysical Morphology, vol 2, (Ed. Glick D). Wiley, New York, 247–282 (1975)

Staehelin L A, Bertrand W S: Temperature and contamination dependent freeze-etch images of frozen water and glycerol solutions, J Ultrastr Res 37, 146–168 (1971)

Steere R L, Erbe E F: Comparison of acrylamide and agar gels by freeze etching. Proc EMSA 35, 606–607 (1977)